

A High-Energy Study of the Geminga Pulsar

M. S. Jackson, J. P. Halpern, and E. V. Gotthelf

Department of Astronomy, Columbia University, New York, NY, 10025-6601

J. R. Mattox

Department of Physics & Astronomy, Francis Marion University, Florence, SC 29501-0547

ABSTRACT

We present the results of deep X-ray and γ -ray observations of the Geminga pulsar obtained in the final years of the *ASCA* and *CGRO* missions, and an upper limit from *RXTE*. A phase-connected ephemeris from the γ -rays is derived that spans the years 1973–2000, after allowing for a minor glitch in frequency of $\Delta f/f = 6.2 \times 10^{-10}$ in late 1996. *ASCA* observations of the hard X-ray pulse profile in 1994 and 1999 confirm this glitch. An improved characterization of the hard X-ray pulse profile and spectrum from the long *ASCA* observation of 1999 confirms that there is a non-thermal X-ray component that is distinct from the γ -ray spectrum as measured by EGRET. It can be parameterized as a power-law of photon index $\Gamma = 1.72 \pm 0.10$ with a flux of 2.62×10^{-13} ergs cm⁻² s⁻¹ in the 0.7–5 keV band and pulsed fraction 0.54 ± 0.05 , similar to, but more precise than values measured previously. An extrapolation of this spectrum into the energy band observed by the *RXTE* PCA is consistent with the non-detection of pulsed emission from Geminga with that instrument. These results are interpreted in the context of outer-gap models, and motivations for future X-ray observations of Geminga are given.

Subject headings: pulsars: individual (Geminga)— stars: neutron — X-rays: stars

1. Introduction

Discovered in 1972 by the SAS-2 satellite (Fichtel et al. 1975; Thompson et al. 1977), Geminga is the second brightest γ -ray source in the sky above 100 MeV (Swanenburg et

al. 1981). It was known only as a γ -ray source until a promising candidate was detected in X-rays by the Einstein Observatory (Bignami, Caraveo, & Lamb 1983), and associated with an optical counterpart (Bignami et al. 1987; Halpern & Tytler 1988; Bignami et al. 1988). Subsequently, Geminga was found to be a rotation-powered pulsar with a period of 237 ms in X-rays by *ROSAT* (Halpern & Holt 1992), and in γ -rays by the Energetic Gamma Ray Experiment Telescope (EGRET) on the *Compton Gamma-ray Observatory* (Bertch et al. 1992). Prior to the discovery of the 237 ms spin period of Geminga, claims had been made for various periods in the range 59–60 s in γ -rays and in X-rays (Thompson et al. 1977; Masnou et al. 1977; Zyskin & Mukanov 1983; Bignami, Caraveo, & Paul 1984; Zyskin 1988; Kaul et al. 1985), but no such detections have been made in high quality X-ray and γ -ray observations during the past decade.

The optical spectrum of Geminga is predominantly non-thermal, with possible ion cyclotron features (Martin, Halpern, & Schiminovich 1998; Mignani, Caraveo, & Bignami 1998). Shearer et al. (1998) reported optical modulation from Geminga that resembles its γ -ray light curve. Geminga is unusual as a rotation-powered pulsar because it is not a strong radio source. In 1997, three groups (Malofeev & Malov 1997; Kuz'min & Losovskii 1997; Shitov & Pugachev 1997) claimed detection of pulsed radio emission at 102 MHz, but observations at other radio frequencies have so far been negative (Ramachandran, Deshpande, & Indrani 1998; McLaughlin et al. 1999; Burderi, Fauci, & Boriakoff 1999; Kassim & Lazio 1999). A phase-connected ephemeris covering the first 27 years of γ -ray observations of Geminga was presented and updated by Mattox, Halpern, & Caraveo (1998, 2000).

In this paper we present the results of a long observation with the *Advanced Satellite for Cosmology and Astrophysics* (*ASCA*), which allows us to better constrain the hard X-ray spectrum of Geminga and perform pulse-phase spectroscopy. X-ray pulse times of arrival are compared with the latest ephemeris from EGRET. Additional constraints on the hard X-ray emission are derived from an observation by the *Rossi X-ray Timing Explorer* Proportional Counter Array (*RXTE* PCA).

2. Observations

A log of the observations used in this paper is given in Table 1. A six-day observation of Geminga was obtained by *ASCA* in 1999 October 5–11. Observations by *RXTE* were made in 1996 April and May. EGRET made many γ -ray observations of Geminga since 1991, until *CGRO* was de-orbited in 2000. We also make brief use of a 1993 *ROSAT* observation of Geminga and a 1994 observation by *ASCA*, both of which were described in detail in Halpern & Wang (1997).

The *ASCA* satellite (Tanaka, Inoue, & Holt 1994) incorporates four co-aligned focal plane detectors, two Gas Imaging Spectrometers (GIS) and two Solid-State Imaging Spectrometers (SIS). Each instrument is positioned at the focus of a conical foil mirror. The SIS instrument is sensitive to X-rays with energies between 0.4 and 10 keV and the GIS detects X-rays between 0.7 and 10 keV. Only the GIS has time resolution sufficient to study the pulsations of Geminga. The 1999 observation was designed with bit assignments such that the time resolution was 0.49 ms in high bit rate telemetry mode, and 3.91 ms at medium bit rate. This required the sacrifice of two bits from the pulse-height analyzer resulting in 256 energy channels instead of the default 1024, and elimination of the five bits of rise-time information; both of these have negligible effect on the quality of the data. The GIS high and medium bit rate data were combined for the timing and spectral analysis. The small amount of low bit rate data in the GIS were not used. For the spectral analysis, data from both the GIS and SIS instruments were used. The SIS observations were conducted in 1-CCD mode.

RXTE (Bradt, Rothschild, & Swank 1993) consists of the Proportional Counter Array (PCA), High Energy X-ray Timing Experiment (HEXTE), and the All Sky Monitor (ASM). The PCA consists of five xenon filled proportional counters, coaligned and collimated, that observe a roughly circular field with $\approx 1^\circ$ FWHM response (Jahoda et al. 1996). The RXTE data analyzed here are exclusively from the PCA, because of its large collecting area (~ 6500 cm² at 10 keV). The PCA data are of interest to search for pulsed emission at higher X-ray energies than *ASCA*, since the PCA is sensitive to X-rays with energies between 2 and 60 keV.

EGRET is a high-energy γ -ray telescope which is sensitive in the energy range from about 30 MeV to 30 GeV. It measures the energy of incoming γ -rays with a NaI(Tl) crystal, and their direction with a multilevel thin-plate spark chamber system which converts the gamma-rays and determines the trajectories of the resulting e^\pm pair, and a triggering telescope that detects the presence of a pair having the correct direction of the motion. An anti-coincidence scintillation dome discriminates against charged particles. EGRET's effective area is ≈ 1000 cm² at 150 MeV, 1500 cm² around 0.5 – 1 GeV, decreasing gradually at higher energies. We used all of the > 100 MeV photons detected by EGRET from Geminga between 1991 and 1997 to make a mean light curve. The event selection is described in Mattox, Halpern, & Caraveo (1998).

3. Timing Analysis

3.1. The Drifting EGRET Ephemeris

Gamma-ray timing provides the most precise and continuous rotational ephemeris of Geminga because of the sharpness of its γ -ray peaks and the large number of observations that have been performed over the years. Combined analysis of EGRET data up to 1997, and earlier data from the *COS B* satellite, yielded a phase-connected, cubic ephemeris (Mattox, Halpern, & Caraveo 1998) that fitted the rotational phase of Geminga for 24 years with residuals smaller than 0.05 cycles (the “1997 ephemeris”). We reproduce this ephemeris in Table 2. The residuals from this timing solution were fitted by Mattox, Halpern, & Caraveo (1998) to a sinusoidal term of semiamplitude 0.026 cycles, possibly attributable to an orbiting planet, but it is now apparent that this was simply a manifestation of timing noise. Beginning in 1997, the phase measured by EGRET began to deviate systematically from the pre-1997 ephemeris in the sense that the peaks arrive earlier than expected (Mattox, Halpern, & Caraveo 2000).

Figure 1 shows the phase residuals of all of the EGRET observations relative to the 1997 ephemeris. The points in Figure 1 correspond to the numbered EGRET epochs in Table 1, some of which were grouped together. According to a fit of the light curves to Lorentzians, described in Mattox, Halpern, & Caraveo (1998), in 1998 July, the gamma-ray peaks were observed to arrive 0.14 ± 0.02 of a cycle earlier than predicted; in 1999 May they arrived 0.22 ± 0.01 cycles early; in 1999 September they arrived 0.24 ± 0.06 cycles early; and during the final EGRET observation in 2000 April–May, the gamma-ray peaks arrived 0.29 ± 0.01 cycles early. This departure from the phase predicted by the 1997 ephemeris is consistent with a minor glitch (discontinuous change in frequency) shortly after the time of the 1996 measurement, MJD ≈ 50382 (1996 Oct. 26), by an amount $\Delta f/f = 6.2 \times 10^{-10}$. By fitting the phase residuals in Figure 1, we derive an approximate post-glitch ephemeris, also given in Table 2. Hereafter, we refer to the “EGRET ephemeris” as the two cubic segments covering the years 1991–2000 in Table 2, plus the residuals from the cubic terms that are illustrated in Figure 1. In the following analysis, we interpolate the EGRET ephemeris, including its phase residuals, in order to phase-align and compare pulse profiles from X-ray wavelengths.

3.2. ASCA Observation

All of the event times in the *ASCA* GIS observation of 1999 October were first converted to Barycentric Dynamical Time (TDB) using the position and proper motion of Geminga listed in Table 2. This was done using the “timeconv” program, which is part of the FTOOLS

software package.

We determined optimal radii for the source extraction and background annulus in the GIS by maximizing the signal-to-noise ratio in the resulting light curve. As shown in Figure 2, the radius of the source circle was chosen to be $3'$, and a concentric annulus of inner and outer radii of $5'$ and $6.25'$, respectively gave a good estimate of the background. We confirm that, as found by Becker et al. (1999) using previous *ROSAT* and *ASCA* images, there is no evidence for diffuse emission (synchrotron nebulosity) associated with Geminga.

In Figure 3 we compare the resulting 0.5–4.0 keV light curve with the only previous hard X-ray light curve of Geminga made with the same instrument in 1994 March and described by Halpern & Wang (1997). The curves have been aligned according to the EGRET ephemeris, and the resulting agreement in phase confirms the drifting EGRET ephemeris shown in Figure 1. To evaluate whether the pulse shape experienced any change between the 1994 and 1999 *ASCA* observations, the two light curves in Figure 3 were compared using χ^2 test, after accounting for the difference in the exposure times. It was determined that the light curves do not differ significantly. The stability of the light curve, and its large pulsed fraction and strong main peak allow the possibility of continuing the rotational ephemeris of Geminga using hard X-ray observations, e.g., with *XMM-Newton* and *Chandra*, during the current epoch in which there are no high-energy γ -ray instruments in orbit.

Figure 4 shows the folded light curves for the 1999 GIS data divided into three energy bands, 0.7 – 1.5 keV, 1.5 – 3.5 keV, and 3.5 – 7.0 keV. For comparison, we also reproduce soft X-ray pulse profiles from a 1993 September observation with the *ROSAT* PSPC that was published by Halpern & Wang (1997), in energy bands 0.08 – 0.28 keV, 0.28 – 0.53 keV, and 0.53 – 1.50 keV. The summed EGRET light curve above 100 MeV is also shown. For CGRO viewing period 1, comparing the number of events selected with $E > 100$ MeV to the likelihood estimate of Geminga flux (Mattox, Halpern, & Caraveo 1996) 63% of the events selected are estimated to be from Geminga. The remaining 37% would be primarily diffuse Galactic gamma-ray emission. This is the estimated background for the EGRET lightcurve. It is statistically consistent with the claim in Mayer-Hasselwander et al. (1994) that there is negligible unpulsed emission from Geminga in that energy band. These light curves resemble closely those given in Figure 9 of Halpern & Wang (1997). Because the 1999 GIS observation had 2.5 times more exposure time than the 1994 observation, the GIS light curves could be split into smaller energy bands, yielding more information about the change in pulse profile from low to medium X-ray energies than was available before. It was clear from the analysis of Halpern & Wang (1997) that thermal surface emission, fitted with $T_{\text{BB}} = (5.6 \pm 0.5) \times 10^5$ K, dominates the X-ray emission below 0.7 keV, whereas the *ASCA* GIS, which is sensitive above 0.7 keV, sees primarily non-thermal emission (see also

§4). The large pulsed fractions of the light curves above 0.7 keV bear out this interpretation. In addition, it was noted in Halpern & Wang (1997) that the non-thermal pulse component itself has energy dependent structure, in particular, an offset of 0.1 cycles between the 0.7 – 1.5 keV PSPC and 1.0 – 4.0 keV GIS light curves. Figures 3 and 4 confirm that the GIS light curve leads the hardest PSPC band (0.53 – 1.50 keV) by approximately 0.1 cycles. However, since the energy resolution of the PSPC is so poor, it is possible that some soft photons of thermal origin bias this light curve’s peak toward later times.

The non-thermal X-ray pulse as illustrated in Figures 3 and 4 is best described as a single broad peak centered at phase 0.63, approximately coinciding with the smaller of the two EGRET peaks, with a possible minor peak at phase 0.97. At the highest energy (> 3.5 keV), the GIS light curve may begin to resemble the EGRET peaks in having two peaks separated by 0.5 cycles, but the statistics are poor and, even if real, the GIS peaks lead the EGRET peaks by ~ 0.1 cycles. On balance, the differences between the GIS and EGRET light curves seem greater than their similarities, and we regard this as evidence that the hard X-rays are not simply an extension of the γ -ray spectrum (see also §4).

3.3. RXTE Observation

The PCA instrument on RXTE was used to search for pulsed emission from 2 – 60 keV. The data were recorded in Good Xenon mode and processed using standard methods. The time resolution for the observation of $0.95\mu\text{s}$ and absolute clock precision of $5\mu\text{s}$ are more than adequate to distinguish pulsations from Geminga. The energy information was stored in eight bits in the event word, and the energy-channel conversion table for Cycle 3 was used to convert to energy in keV.

The barycenter-corrected PCA data in the energy ranges 2–15 keV and 15–60 keV were folded using the EGRET ephemeris. The faseBin routine, an epoch folding test, a Fourier transform pulse search, a Rayleigh test (Leahy, Elsner, & Weisskopf 1983), and the Z_n^2 test of orders 2 and 3 (Buccheri et al. 1983) were performed on the data. No significant pulsations were detected using any of these techniques in the energy range in which pulsations were detected by *ASCA*, nor at higher energies, with a flux upper limit of 3.5×10^{-13} ergs cm^{-2} s^{-1} in the 2 – 15 keV energy range. This negative result is undoubtedly due to the high background that dominates in this non-imaging instrument, in combination with spectral shape of Geminga’s non-thermal emission, as will be discussed in the next section.

4. Spectral Analysis

4.1. ASCA X-ray Spectrum

The FTOOLS/XSELECT software package was used to prepare the *ASCA* data for spectral analysis. Source spectra were extracted from a circle 2'5 in radius for the SIS data, and 3'5 in radius for the GIS data. The source was at a suitable location for background spectra to be extracted from annuli concentric with the source circle for both SIS and GIS. It is important to choose an annulus close enough to the source circle to acquire a fair sample of the background sky at the point of the source, but not close enough to contain a significant number of source counts, which would oversubtract the source spectrum.

To obtain response matrices, the latest GIS “rmf” files were downloaded and rebinned to match the reduced number of energy channels in the data. The “sisrmg” program was used to generate response matrices (rmfs) for the SIS spectral files. Ancillary response (arf) files were created from the rmf files using the program “ascaarf”. The spectral data were rebinned, using the program “grppha” so that there were 40 counts or more in each bin. This reduces the noise, especially at higher energies where the instrument has less sensitivity, and allows Gaussian statistics to be used in the evaluation of the fit.

Guided by the combined *ROSAT/ASCA* results of Halpern & Wang (1997), we fitted simple power-law models to each of the *ASCA* instruments using XSPEC. The soft blackbody component that dominates the *ROSAT* spectrum does not contribute significantly in the *ASCA* band, and was neglected. In this analysis, the intervening column density N_{H} was held fixed at the best fitted value of 1.07×10^{20} given in Halpern & Wang (1997). Uncertainties in this small N_{H} do not affect the *ASCA* results. The energy limits of the fit for the SIS data were set at 0.7 – 10 keV for SIS0, and 0.7 – 7.5 keV for SIS1 data because of its poorer signal-to-noise at higher energy. The GIS spectra were fitted from 0.8 – 10 keV to avoid calibration uncertainties at the lowest energies. In addition to fits of the individual instruments, combined fits were made. The combined SIS and GIS fits are shown in Figures 5 and 6.

Results of the fits are given in Table 3 for the combined SIS and GIS as well as for all instruments combined. All fits are acceptable, with $\chi^2 \sim 1$ per degree of freedom. Although not all of the instruments are consistent with each other at the 68% confidence level, three out of four are consistent with the combined SIS+GIS fit, which yields photon index $\Gamma = 1.72_{-0.09}^{+0.10}$. This compares favorably with the lower-quality results of Halpern & Wang (1997), who found $\Gamma = 1.47_{-0.23}^{+0.25}$ for SIS0 and $\Gamma = 2.19_{-0.31}^{+0.35}$ for GIS3 in the 1994 observation.

We also performed crude pulse-phase spectroscopy by separating the GIS events into two phase bins, 0.28–0.88 in Figures 3 and 4 (which includes most of the main peak), and the remainder (0.88–0.28). Power-law fits in the range 0.8 – 8.0 keV were performed for both sets, and the results are also listed in Table 3. While the spectrum of the main peak is slightly softer than that of the interpeak region ($\Gamma = 2.00 \pm 0.24$ vs. $\Gamma = 1.74 \pm 0.24$), the difference is only marginally significant.

Table 3 also gives the modeled fluxes in the range 0.7 – 5.0 keV, normalized to a full cycle. The fluxes for the full data sets are similar to those for the PSPC+SIS0 fit given in Halpern & Wang (1997), but are more than twice the flux in the PSPC+GIS3 fit given there. The fluxes for the individual instruments in our 1999 *ASCA* observation agree with each other quite well, with the GIS tending to show a slightly higher flux than the SIS. We conclude that the discrepancies between SIS and GIS spectra in the 1994 observation noted by Halpern & Wang (1997) were largely due to the shorter exposure and non-optimal mode of that observation, while the current results from the 1999 observation are more internally consistent and precise.

4.2. Broad-band Spectrum of Geminga

An updated broad-band spectrum of Geminga, including the new data presented in this paper, is shown in Figure 7. The previous sources for data and upper limits are given in the Figure caption. We derived upper limits from *RXTE* for the pulsed flux by determining the minimum pulsed detection threshold for the Z_n^2 test (which should provide the greatest sensitivity of all Z_n^2 tests, for a pulse shape similar to the hard X-ray or γ -ray pulse profile in Figure 4) and the epoch folding test. The frequency at the epoch of the observation is well-defined by the EGRET ephemeris (i.e., a search over frequency is not required, although we nevertheless performed a search in a small frequency range immediately surrounding the expected value), and the pulse shape can be approximated by a sine wave. Using the appropriate parameters similar to those in Leahy, Elsner, & Weisskopf (1983) for the epoch folding test (which, for a pulse shape like that at the highest energy observed by *ASCA* has the lowest pulsed detection threshold), we derived upper limits for 10 and 60 keV corresponding to the collecting area of the PCA under the assumption of a power-law of $\Gamma = 1.72$ as measured by *ASCA*. It is apparent from Figure 7 that, given its flux and spectral index, Geminga is too faint for its pulsed flux to have been detected at any energy by the *RXTE* PCA instrument.

5. Interpretation

It is clear from Figure 7 that the γ -ray emission from Geminga represents the energetically dominant component of the total emission of the pulsar, while an extrapolation of the nonthermal X-ray spectrum falls well below the EGRET flux. The hard X-rays therefore represent a physically distinct emission mechanism from the primary γ -rays. A general theory of X-ray emission from rotation-powered pulsars (Wang, et al. 1998) predicted that any strong γ -ray pulsar will also have a hard X-ray spectrum with photon index $\Gamma = 1.5$. In this model, an outer-gap accelerator will send e^\pm pairs flowing inward and outward along open magnetic field lines. These particles continuously radiate γ -rays by the curvature mechanism. When the inward flowing particles approach the surface of the star, the > 100 MeV γ -rays that they emit convert into secondary e^\pm pairs in the inner magnetosphere wherever $B \sin\phi > 2 \times 10^{10}$ G, where ϕ is the angle between the photon and the \mathbf{B} field. Those secondary pairs must radiate away their energy instantaneously in the strong local \mathbf{B} field. Such a synchrotron decay spectrum has $\Gamma = 1.5$ between ~ 0.2 keV and 5 MeV. The luminosity of such a component in the *ASCA* bandpass is estimated theoretically from the Goldreich-Julian current in the outer-gap accelerator, and is found to be $\sim 1 \times 10^{30}$ ergs s^{-1} , in agreement with the observed flux from Geminga.

A three-dimensional magnetosphere model of Geminga with a thick outer gap is presented by Zhang & Cheng (2001), who explain the phasing of the soft and hard X-ray emission with respect to the γ -ray pulse profile as observed by Halpern & Wang (1997). Their modeled hard X-ray peak coincides with the first γ -ray peak as a result of the inward motion of the X-ray synchrotron emitting particles, while the soft, thermal X-ray peak coming from near the polar cap coincides with the second γ -ray peak. Zhang & Cheng (2001) fitted the γ -ray pulse profiles with a magnetic inclination angle of $\sim 50^\circ$ and a viewing angle of $\sim 86^\circ$, which would also be compatible with the pulse modulation of the soft X-rays.

While the fitted *ASCA* spectral index of $\Gamma = 1.72 \pm 0.10$ does not strongly support or refute this theory, it can be noted that a power-law fit is merely a parameterization of the shape of the X-ray spectrum that does not allow for possible complications due to additional processes that may be occurring. For example, the cyclotron energy for electrons in the pulsar's inner magnetosphere is in the *ASCA* bandpass, which means that the cyclotron spectrum must deviate from a power law there. The nonthermal spectrum must turn down at low energies, both from theoretical arguments, and empirically in order not to exceed the observed ultraviolet and visible flux. Furthermore, it is possible that there is an additional, hotter thermal component around 1 keV which would arise from the polar caps heated by the impacting charged particles flowing in along the open field lines, such as in the model of Perna, Heyl, & Hernquist (2001). The latter model was based on double-

blackbody fits to the *ROSAT* spectrum alone, taken from Halpern & Ruderman (1993), but since superseded by evidence from *ASCA* that the harder component is non-thermal (Halpern & Wang 1997). Nevertheless, it is still possible that a fainter, hot thermal component is present that is not easily distinguished from the dominant non-thermal spectrum and pulse profiles, but that contaminates the power-law fit. Our pulse-phase spectroscopy, even in the long *ASCA* observation of 1999, is not sensitive enough to meaningfully constrain such a complex model. The detection of X-rays above 10 keV from Geminga is an unmet challenge, but one that might be necessary to better measure the the predicted power-law spectrum.

6. Final Remarks

We were startled to see a recent report of detection of a 62 s period from Geminga in TeV γ -rays (Neshpor & Stepanyan 2001). That paper cited nine other detections of periods in the range 59–60 s (see §1 for references), going all the way back to analyses of *SAS 2*, *COS B*, *Einstein*, and *EXOSAT* data, none of which was ever considered convincing (Buccheri et al. 1985). We have searched *ROSAT* and *ASCA* data in this range of periods without detecting significant modulation. For example, there is no signal at a period of 62.4 s that would fit the linear extrapolation of previous claims to the *ASCA* observation of 1999. We regard the case of the moving 60 s period as closed a decade ago, notwithstanding this recent attempt at revival.

Although there is no γ -ray telescope currently in orbit, it will be possible to maintain a phase-connected ephemeris and monitor Geminga’s glitch activity using X-ray instruments such as *Chandra* and *XMM-Newton*, now that we have confirmed the precise phase relationship between the hard X-ray and γ -ray pulse in two *ASCA* observations. The standard dipole braking index $n = \ddot{f}f/\dot{f}^2 = 3$ would correspond to \ddot{f} smaller than the observed value by a factor of 5.5. Despite the existence of a 27 yr long phase-connected γ -ray ephemeris of Geminga, it has not been possible to measure a true braking index because \dot{f} is apparently dominated by timing noise, even apart from the observed glitch, which is among the smallest ever detected in a pulsar. More sensitive hard X-ray observations, such as are possible with *XMM-Newton*, also have the potential to disentangle any additional spectral and pulse components that may be present, such as cyclotron features, hot polar cap emission, and even atomic spectral lines from the neutron star photosphere.

REFERENCES

Akerlof, C. W., et al. 1993, *A&A*, 274, L17

- Becker, W., Kawai, N., Brinkmann, W., & Mignani, R. 1999, *A&A*, 352, 532
- Bertch, D. L., et al. 1992, *Nature* 357, 306
- Bignami, G. F., Caraveo, P. A., & Lamb, R. C. 1983, *ApJ*, 272, L9
- Bignami, G. F., Caraveo, P. A., & Paul, J. A. 1984, *Nature*, 310, 464
- Bignami, G. F. et al. 1987 *ApJ*, 319, 358
- Bignami, G. F., Caraveo, P. A., & Paul, J. A. 1988, *A&A*, 202, L1
- Bignami, G. F., et al. 1996, *ApJ*, 456, L111
- Bradt, H. V., Rothschild, R. E., & Swank, J. H. 1993, *A&AS*, 97, 355
- Buccheri, R., et al. 1983, *A&A*, 128, 245
- Buccheri, R., D’Amico, N., Hermsen, W., & Sacco, B. 1985, *Nature*, 316, 131
- Burderi, L., Fauci, F., & Boriakoff, V. 1999, *ApJ*, 512, L59
- Caraveo, P. A., Lattanzi, M. G., Massone, G., Mignani, R. P., Makarov, V.V., Perryman, M. A. C., & Bignami, G. F. 1998, *A&A*, 329, L1
- Fichtel, C. E. et al. 1975, *ApJ*, 198, 163
- Fierro, J. M., et al. 1998, *ApJ*, 494, 794
- Halpern, J. P., & Holt, S. S. 1992, *Nature*, 357, 222
- Halpern, J. P., & Ruderman, M. 1993, *ApJ*, 415, 286
- Halpern, J. P., & Tytler, D. 1988, *ApJ*, 330, 201
- Halpern, J. P., & Wang, F. Y.-H. 1997, *ApJ*, 477, 905
- Jahoda, K., et al. 1996, *Proc. SPIE*, 2808, 59
- Kassim, N. E., & Lazio, T. W. 1999 *ApJ*, 527, L101
- Kaul, R. K., et al. 1985, in *Proc. 19th Int. Cosmic Ray Conf. (La Jolla)*, 1, 165
- Kuiper, L., et al. 1996, *A&A*, 120, 73
- Kuz’min, A. D., & Losovskii, B. Ya. 1997, *Astronomy Letters*, 23, 323

- Leahy, D. A., Elsner, R. F., & Weisskopf, M. C. 1983, *ApJ*, 272, 256
- Malofeev, V. M., & Malov, O. I. 1997, *Nature*, 389, 697
- Martin, C., Halpern, J. P., & Schiminovich, D. 1998 *ApJ*, 494, L211
- Masnou, J. L., et al. 1977, *Proc. 12th ESLAB Sym. (Frascati)*, p. 33
- Mattox, J. R., Halpern, J. P., & Caraveo, P. A. 2000, *A&AS*, 120, 77
- Mattox, J. R., Halpern, J. P., & Caraveo, P. A. 1998, *ApJ*, 493, 891
- Mattox, J. R., Halpern, J. P., & Caraveo, P. A. 2000, *BAAS*, 197, #130.05
- Mayer-Hasselwander, H. A., et al. 1994, *ApJ*, 421, 276
- McLaughlin, M. A., Cordes, J. M., Hankins, T. H., & Moffett, D. A. 1999, *ApJ*, 512, 929
- Mignani, R. P., Caraveo, P. A., & Bignami, G. F. 1998, *A&A*, 332, L37
- Neshpor, Yu. I., & Stepanyan, A. A. 2001, *Astronomy Letters*, 27, 794
- Perna, R., Heyl, J., & Hernquist, L. 2001, *ApJ*, 553, 809
- Ramachandran, R., Deshpande, A. A., & Indrani, C. 1998, *A&A*, 339, 787
- Schroeder, P. C., et al. 1995, *ApJ*, 450, 784
- Shearer, A., et al. 1998, *A&A*, 335, 21
- Shitov, Yu. P., & Pugachev, V. D. 1997, *New Astronomy* 3 (2), 101
- Swanenburg, B. N. et al. 1981 *ApJ*, 243, L69
- Tanaka, Y., Inoue, H., & Holt, S.S. 1994, *PASJ*, 46, L37
- Thompson, D. J., Fichtel, C. E., Hartman, R. C., Kniffen, D. A., & Lamb, R. C. 1977, *ApJ*, 213, 252
- Wang, F. Y.-H., Ruderman, M., Halpern, J. P., & Zhu, T. 1998, *ApJ*, 498, 373
- Zhang, L., & Cheng, K. S. 2001, *MNRAS*, 320, 477
- Zyskin, Y. I., & Mukanov, D. B. 1983, *Sov. Astron. Lett*, 9, 117
- Zyskin, Y. I. 1988, *Space Sci. Rev.*, 49, 49

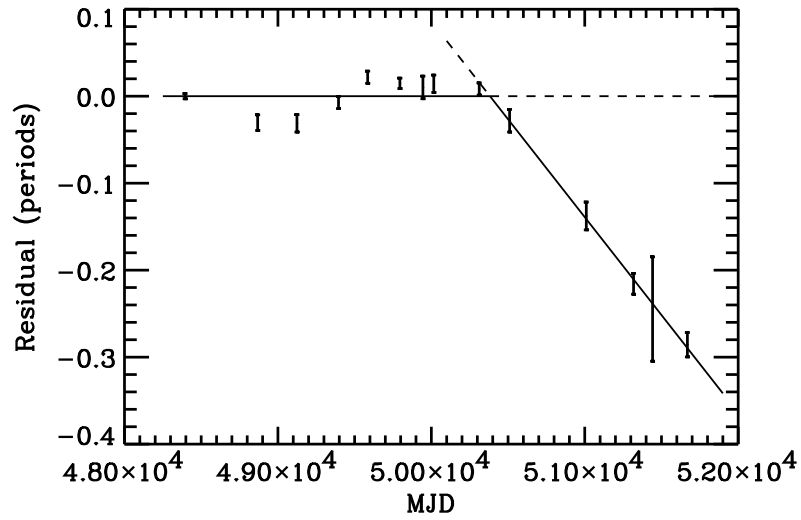


Fig. 1.— Phase residuals of the EGRET timing observations of Geminga relative to the cubic “1997 ephemeris” of Mattox, Halpern, & Caraveo (1998) (pre-glitch ephemeris in Table 2). The 14 measurements correspond to the numbered EGRET epochs in Table 1, some of which were grouped together. The *solid line* represents the cubic ephemeris segments before and after the glitch. The post-glitch ephemeris is also given in Table 2.

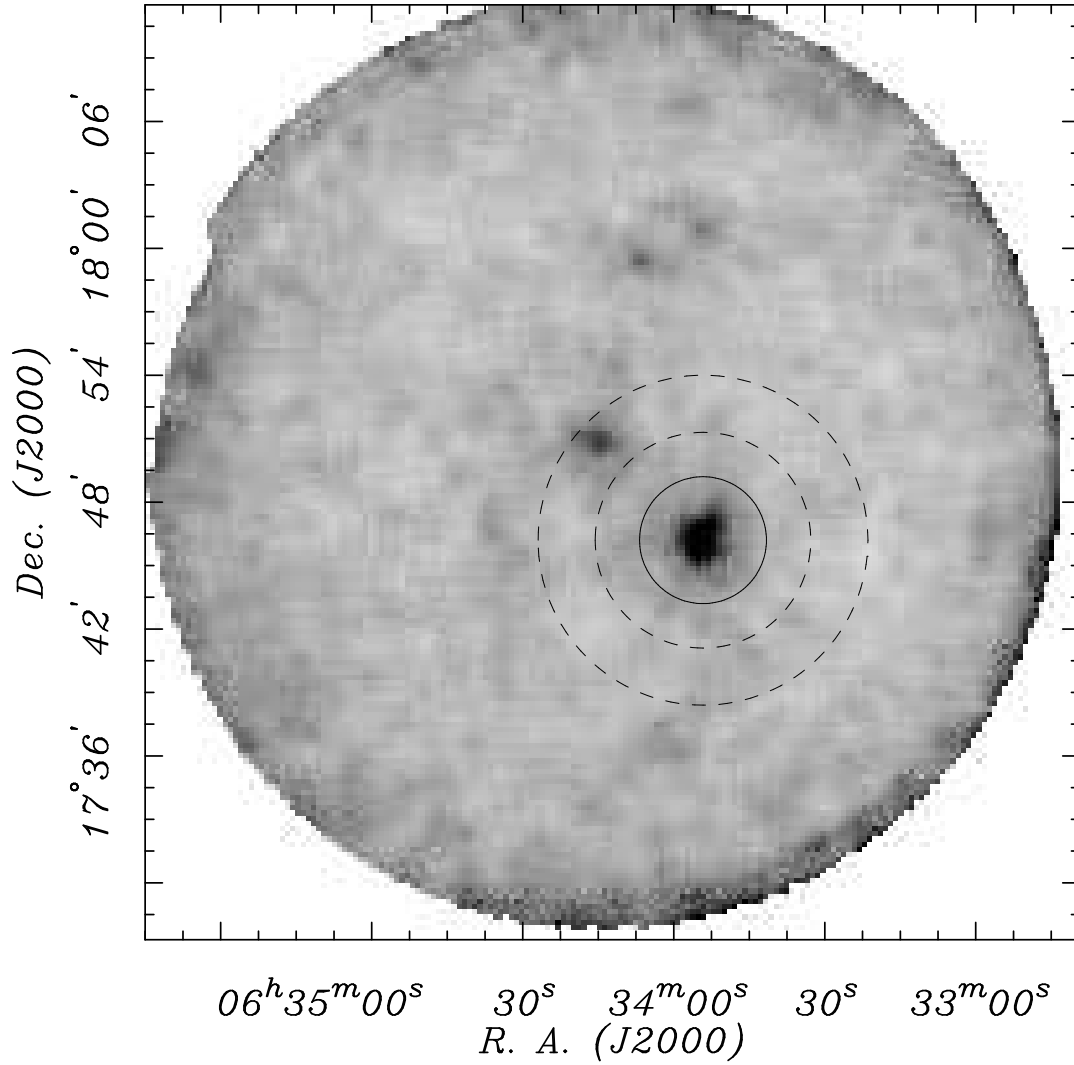


Fig. 2.— *ASCA* GIS image of Geminga, showing the source circle (solid line) and annulus (dashed lines) from which the background was subtracted for calculation of the pulse profile. The radii of the source circle (3′) and background annulus (5′–6′.25) were chosen to maximize the signal-to-noise ratio in the light curve.

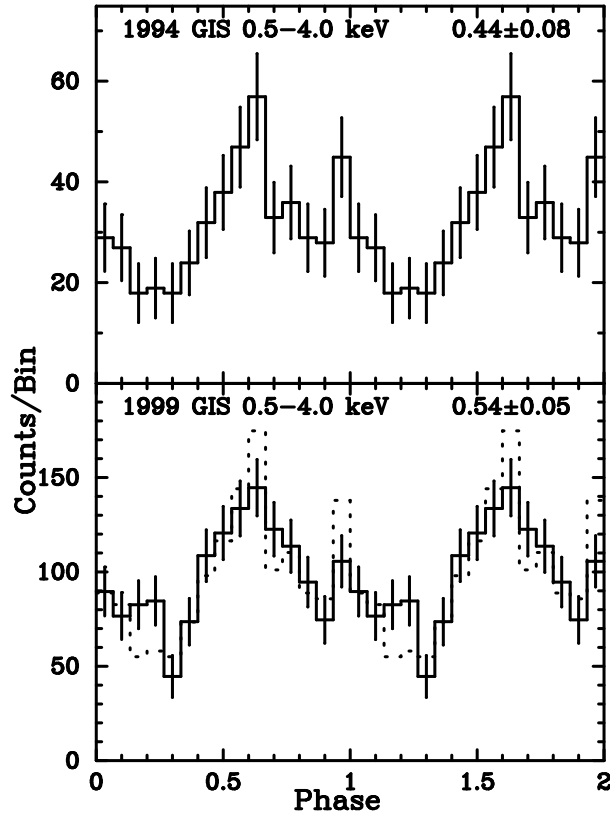


Fig. 3.— Comparison of background-subtracted pulse profiles in the 0.5–4.0 keV band from 1994 and 1999 *ASCA* GIS observations of Geminga. The dashed line is the 1994 light curve normalized to the total counts in the 1999 light curve. Phase zero corresponds to epoch T_0 in Table 2. The pulsed fractions and their uncertainties are indicated in each panel.

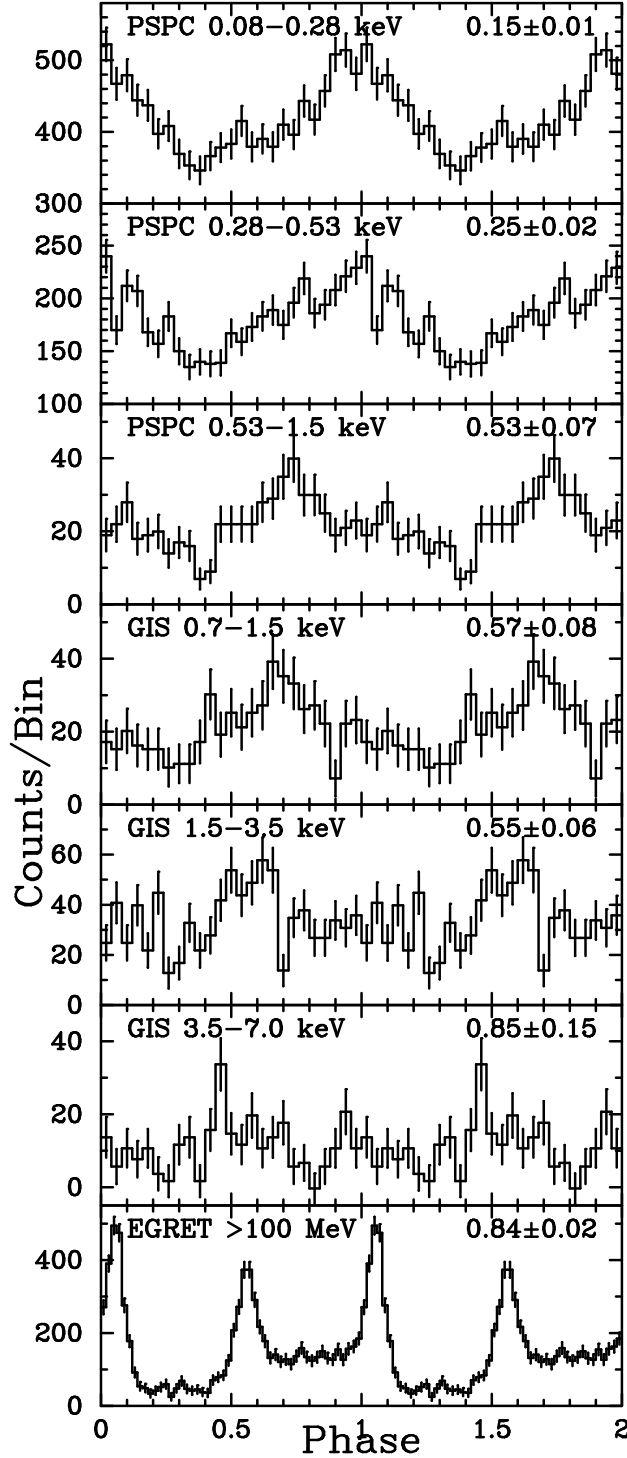


Fig. 4.— Pulse profiles from 1993 *ROSAT* PSPC and 1999 *ASCA* GIS observations of Geminga, along with the summed EGRET light curve, folded at the ephemeris of Table 2. Phase zero corresponds to epoch T_0 in Table 2. The pulsed fractions and their uncertainties are indicated in each panel. Background subtraction of all light curves has been performed. Compare with the similar Figure 9 of Halpern & Wang (1997).

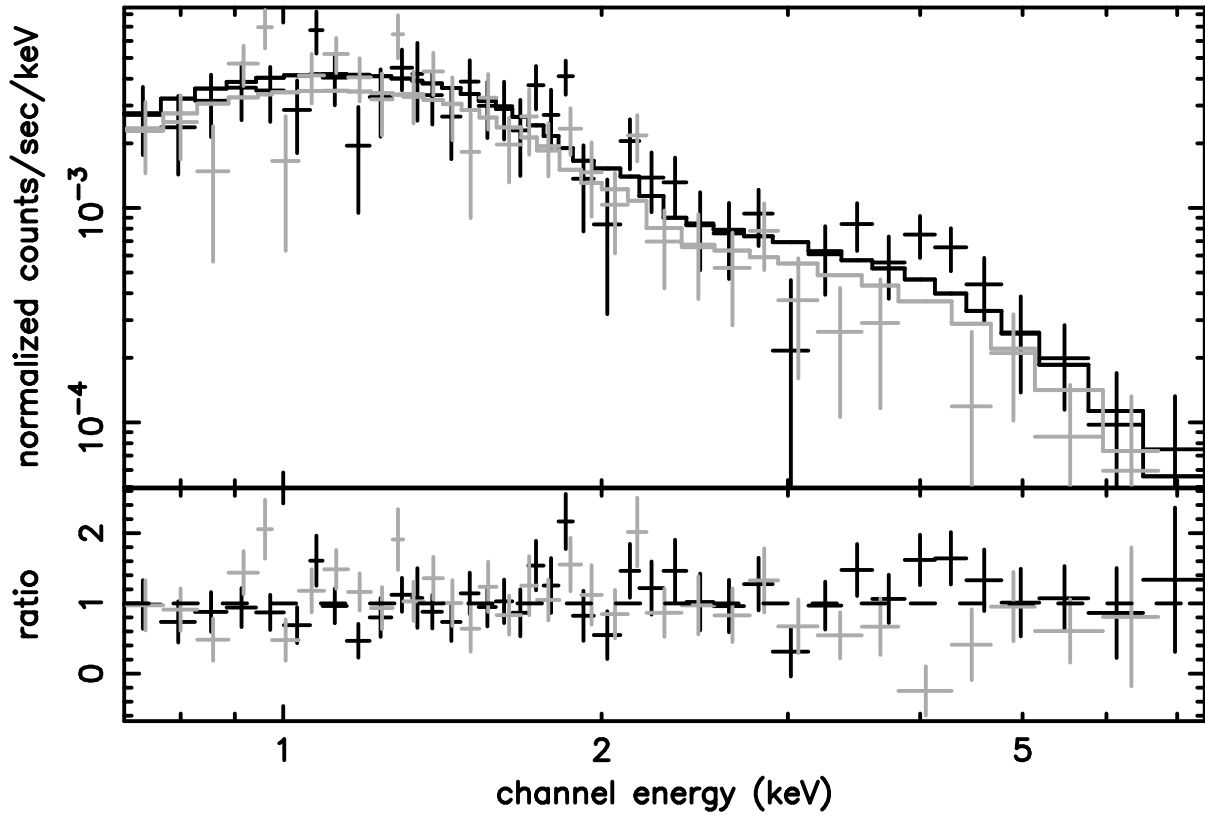


Fig. 5.— Fit of *ASCA* SIS spectra of Geminga to a power law. *Dark line*: The SIS0 data and model; *Light line*: The SIS1 data and model. The lower panel shows the residuals of the data from the model. The fitting parameters are given in Table 3.

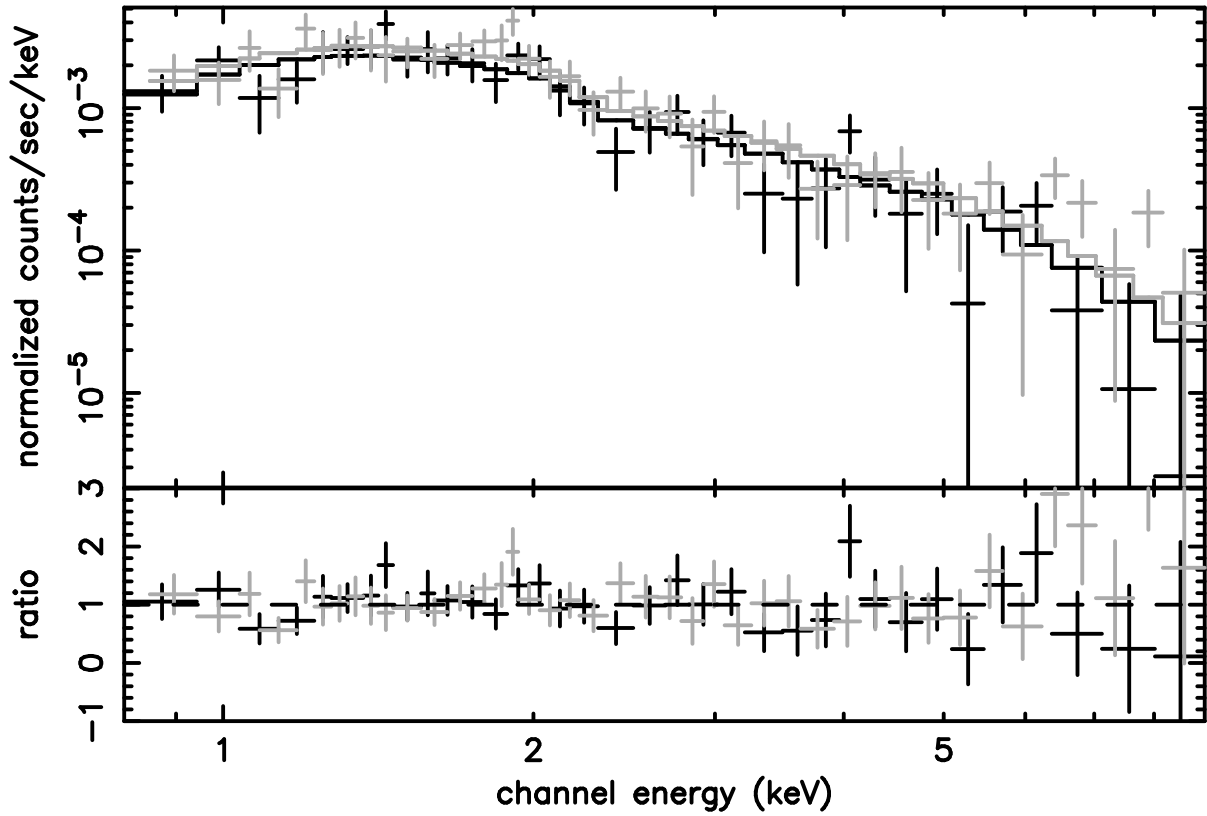


Fig. 6.— Fit of *ASCA* GIS spectra of Geminga to a power law. *Dark line*: The GIS2 data and model; *Light line*: The GIS3 data and model. The lower panel shows the residuals of the data from the model. The fitting parameters are given in Table 3.

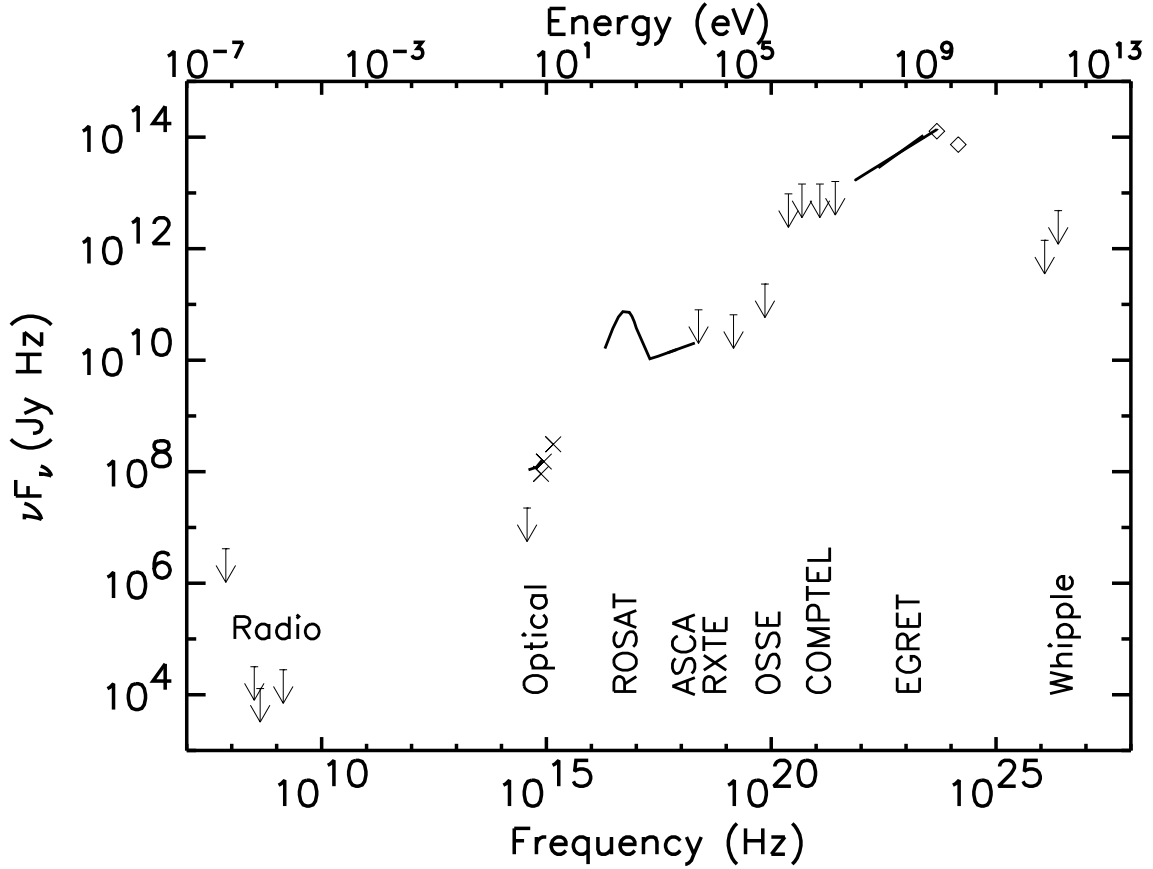


Fig. 7.— The broad-band energy spectrum of Geminga. Upper limits correspond to that of the pulsed flux, whereas the data points represent the total flux. In order of increasing energy, the references are as follows: The upper limits in the radio are found in Burderi, Fauci, & Boriakoff (1999) and Kassim & Lazio (1999). The *I*-band upper limit is from Bignami et al. (1996). The optical spectrum is from Martin, Halpern, & Schiminovich (1998). The UV points (*X*'s) are from Mignani, Caraveo, & Bignami (1998) and Bignami et al. (1996). The curve in the soft X-ray band represents the blackbody plus power-law fit to the *ROSAT* PSPC (Halpern & Wang 1997). The *ASCA* curve represents the power law fitted to the *ASCA* data in this paper. The upper limits at 10 and 60 keV (just above the *ASCA* points) represent the pulsed detection threshold at those energies of the *RXTE* data described in the text, assuming a continuation of the *ASCA* measured power-law index. The upper limit at 300 keV is from OSSE (Schroeder et al. 1995) and the COMPTEL upper limits at 1–11 MeV are from Kuiper et al. (1996). The EGRET γ -ray curves are from Mayer-Hasselwander et al. (1994) and Fierro et al. (1998), respectively, and the points just above the curves are also from Fierro et al. (1998). The VHE upper limits are from Akerlof et al. (1993).

Table 1. Log of Observations

Instrument	Dates	Exposure time (ks)	Count rate (s^{-1})
EGRET (1)	1991 Apr 22–May 7	1209.6	1.8×10^{-3}
EGRET (1)	1991 May 16–30	1209.6	1.6×10^{-3}
EGRET (1)	1991 Jun 8–15	604.8	1.5×10^{-3}
EGRET (2)	1992 Jun 11–25	1209.6	2.2×10^{-4}
EGRET (2)	1992 Aug 11–20	777.6	1.9×10^{-4}
EGRET (2)	1992 Sep 1–17	1382.4	1.7×10^{-4}
EGRET (2)	1992 Oct 8–15	604.8	1.4×10^{-4}
EGRET (2)	1992 Nov 3–17	1209.6	1.0×10^{-4}
EGRET (3)	1993 Mar 23–29	604.8	3.2×10^{-4}
EGRET (3)	1993 May 13–24	950.4	4.1×10^{-4}
EGRET (4)	1993 Dec 1–13	1036.8	3.5×10^{-4}
EGRET (4)	1994 Feb 8–17	777.6	7.7×10^{-4}
EGRET (5)	1994 Aug 9–29	1814.4	3.7×10^{-4}
EGRET (6)	1995 Feb 28–Mar 21	1814.4	4.0×10^{-4}
EGRET (6)	1995 Apr 4–11	604.8	2.5×10^{-4}
EGRET (6)	1995 May 9–Jun 6	2419.2	1.8×10^{-4}
EGRET (7)	1995 Aug 8–22	1209.6	2.4×10^{-4}
EGRET (8)	1995 Oct 17–31	1209.6	2.7×10^{-4}
EGRET (9)	1996 Jul 30–Aug 27	2419.2	3.4×10^{-4}
EGRET (10)	1997 Feb 18–Mar 18	2419.2	1.5×10^{-4}
EGRET (11)	1998 Jul 7–21	1209.6	2.0×10^{-4}
EGRET (12)	1999 May 11–25	1209.6	2.1×10^{-4}
EGRET (13)	1999 Sep 14–28	1209.6	4.7×10^{-5}
EGRET (14)	2000 Apr 25–May 9	1209.6	2.6×10^{-4}
ROSAT PSPC	1993 Sep 16–20	36.9	0.503
ASCA SIS	1994 Mar 28–31	49.2	1.7×10^{-2}
ASCA GIS	1994 Mar 28–31	75.3	1.2×10^{-2}
ASCA SIS	1999 Oct 5–11	194.0	1.4×10^{-2}
ASCA GIS	1999 Oct 5–11	207.8	1.0×10^{-2}
RXTE PCA	1996 Apr 27–May 8	142.7	—

Table 2. The Geminga EGRET Ephemeris

Parameter	Pre-glitch ^a	Post-glitch ^b
Epoch of ephemeris T_0 (MJD) ^c ^d	46599.5	50381.999999364
Range of valid dates (MJD)	41725 – 50382	50382 – 51673
Frequency f (Hz)	4.217705363081(13)	4.21764157512(18)
Frequency derivative \dot{f} (Hz s ⁻¹)	$-1.9521712(12) \times 10^{-13}$	$-1.951684(77) \times 10^{-13}$
Frequency second derivative, \ddot{f} (Hz s ⁻²)	$1.49(3) \times 10^{-25}$	$1.49(3) \times 10^{-25}$
Parameter ^e	Value	
Epoch of position (MJD)	49793.5	
R.A. (J2000)	6 ^h 33 ^m 54 ^s .153	
Decl. (J2000)	+17°46′12″.91	
R.A. proper motion μ_α (mas yr ⁻¹)	138	
Decl. proper motion μ_δ (mas yr ⁻¹)	97	

^aFrom Mattox, Halpern, & Caraveo (1998).

^b \dot{f} and \ddot{f} assumed unchanged at the time of the glitch.

^cMJD=JD-2400000.5

^dEpoch of phase zero in Figures 3 and 4.

^ePosition and proper motion from Caraveo et al. (1998).

Note. — Digits in parentheses following a parameter value indicate ~95% confidence uncertainties in the last digits of the parameter.

Table 3. Power-law Fits to ASCA Spectra

Instrument	Γ (68% conf. errors)	Flux (ergs cm ⁻² s ⁻¹) ^a
SIS	1.68 (+0.13, -0.12)	2.29×10^{-13}
GIS	1.99 (+0.14, -0.14)	2.78×10^{-13}
GIS+SIS	1.72 (+0.10, -0.09)	2.62×10^{-13}
GIS ^b	2.00 (+0.24, -0.24)	3.30×10^{-13}
GIS ^c	1.74 (+0.24, -0.23)	2.71×10^{-13}

^aFlux in the 0.7 – 5.0 keV range, before interstellar absorption. In the case of phase-resolved spectra, the flux has been normalized to a full cycle.

^bPhases 0.28–0.88 in Figures 3 and 4.

^cPhases 0.88–0.28 in Figures 3 and 4.